INFLUENCE OF APEX ANGLE AND NOZZLE DESIGN ON ENERGY AND MOMENTUM TRANSFER DURING THE WATER ATOMIZATION PROCESS

Conference Paper · June 2017

CITATION
1

READS
588

8 authors, including:

Zhonghui Jiao
University of Toronto
2 PUBLICATIONS **15** CITATIONS
SEE PROFILE

Donghui Li
University of Toronto
40 PUBLICATIONS **116** CITATIONS
SEE PROFILE

Ali Asgarian
University of Toronto
22 PUBLICATIONS **26** CITATIONS
SEE PROFILE

Saikat Chatterjee
M. N. Dastur & Company (P) Ltd.
39 PUBLICATIONS **94** CITATIONS
SEE PROFILE

INFLUENCE OF APEX ANGLE AND NOZZLE DESIGN ON ENERGY AND MOMENTUM TRANSFER DURING THE WATER ATOMIZATION PROCESS

Zhonghui Jiao[1], Donghui Li[1] Ali Asgarian[1], Saikat Chatterjee[1],Bruno Girard[2], Vladimir Paserin[2], Francois Lavallee[2], Kinnor Chattopadhyay[1]

1. Department of Materials Science and Engineering, University of Toronto, 184 College Street, Toronto, Ontario M5S 3E4, Canada
2. Rio Tinto Fer et Titane, 1625, route Marie-Victorin, Sorel-Tracy, Quebec, J3R 1M6, Canada

ABSTRACT

The water atomization process is a standard and economical process for steel powder production. However, it faces challenges in attaining control of powder size distribution and especially in reducing oversized fraction. A CFD model was developed to understand the effects of water jet apex angle, and nozzle design on droplet dynamics, energy and momentum transfer, and particle size control. Various apex angles were tested and the energy and momentum transfer from the water jet to the metal stream was plotted. Several nozzle designs were conceptualized and tested through CFD simulations. The effect of the diameter of the metal stream was also evaluated. The present study aided in understanding the fundamentals and applying them to control the powder production process.

1.0 INTRODUCTION

High-pressure water atomization has been used to produce various grades of metal alloy powders for a wide range of applications for the last few decades. A classic example is iron and steel powder for the powder metallurgy industry. Along with the huge potential saving in production costs, producing parts from powder using pressing and sintering techniques also opens up new possibilities for more creative and complex designs, especially in the automotive industry and soon in the additive manufacturing industry.

Water atomization process starts with tapping liquid metal from a ladle to a tundish as shown in Figure 1. The molten metal stream thereafter flows through a ceramic ring-shaped nozzle located at the bottom of the tundish, which allows the liquid steel to enter a V-shape jet water atomizing system guided by the force of gravity. When the stream of liquid metal is hit by jets of highly pressurized water, it is broken into fine droplets. Some droplets freeze immediately into fine metal particles while others grow into small irregularly shaped agglomerates while freezing. After atomization, the wet metal powder is dewatered, dried, screened, homogenized and packaged into special containers for sale or further processing[1].

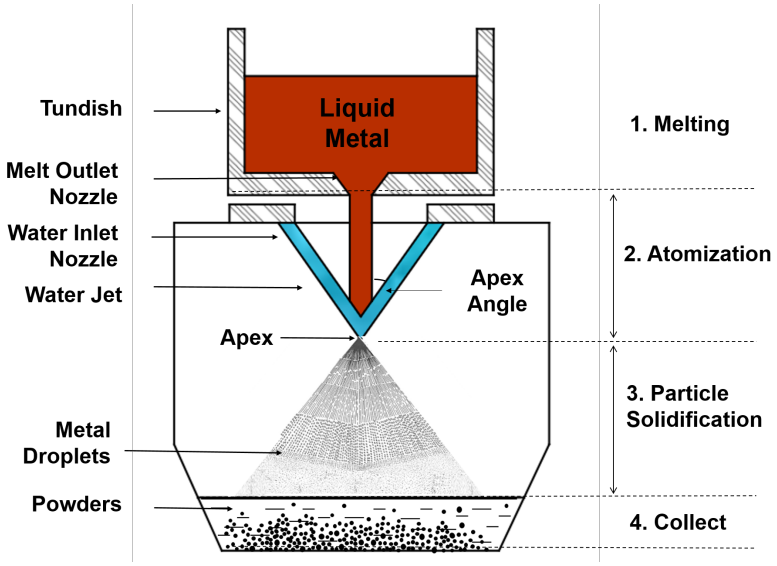

Figure 1. Schematic diagram of water atomization process.

In order for water atomized powder production to remain competitive, an understanding of not only average values of various process parameters, but also variations such as particle size distribution, is vital. In practice, especially at large production scale, a precise control of the particle size is critical in achieving product uniformity and maximizing the production yield since only certain ranges of particles hold commercial values. Previous work has identified various operational parameters towards particle size distribution using both mathematical and experimental methods[2][3][4][5][6][7][8].

Although various process parameters and their influence on particle size distribution have been closely studied through experimental techniques, the effects of apex angle, nozzle design and liquid metal stream diameter on the energy transfer as well as the momentum transfer during atomization are yet to be thoroughly understood. In the present study, a three dimensional mathematical model was developed using ANSYS-FLUENT 16.2. The main objective was to increase our knowledge with regards to the effect of the apex angle, the water nozzle design (i.e. water jet diameter and water flowrate) and the liquid steel inlet diameter on energy and momentum transfer during water atomization of ferrous powders.

2.0 MATHEMATICAL MODELING AND COMPUTATION METHODS

The numerical simulation for the study of apex angle and nozzle design was performed using ANSYS-FLUENT version 16.2. The standard k-ε turbulence model was used to model turbulence, whereas the Eulerian-Eulerian model was used to track liquid steel, water and air interfaces. The various physical properties are depicted in Table I.

Table I: Physical property of liquid steel, water and air used in the present model.

Parameters	Liquid Steel	Water	Air
Density ($kg \cdot m^{-3}$)	7000	998.2	1.225
Viscosity ($kg \cdot m^{-1} \cdot s^{-1}$)	6.000e-3	1.003e-3	1.789e-5

2.1 TURBULENCE MODELING: THE STANDARD k -Ɛ TURBULENCE MODEL

The standard k -ε turbulence model was employed in the present work to model turbulence. More

specifically, ε stands for the rate of turbulence energy dissipation while k is the kinetic energy of turbulence per unit mass and is related to the time-averaged –velocity $\overline{u_i'}$ as follows:

$$k = \frac{1}{2}\sum \overline{u_i'^2} \qquad \text{Equation 1}$$

There are two additional equations for k and ε that need to be solved as follows:

$$\frac{Dk}{Dt} = \frac{\nu_t}{\sigma_k}\nabla^2 k + G_k - \varepsilon \qquad \text{Equation2}$$

$$\frac{D\varepsilon}{Dt} = \frac{\nu_t}{\sigma_\varepsilon}\nabla^2 \varepsilon + \frac{\varepsilon}{k}(C_1 G_k - C_2\varepsilon) \qquad \text{Equation 3}$$

The parameter G_k represents the rate of production of k and is given by the following equation:

$$G_k = \nu_t\left[\frac{\partial u_i}{\partial x_j} + \frac{\partial u_j}{\partial x_i}\right]\frac{\partial u_i}{\partial x_j} \qquad \text{Equation 4}$$

Furthermore, the effective viscosities and the turbulent are calculated based on the following relations:

$$\mu_{eff} = \mu + \mu_t \qquad \text{Equation 5}$$

$$\mu_t = \frac{C_\mu \rho k^2}{\varepsilon} \qquad \text{Equation 6}$$

The values for the constants in the standard k-ε turbulence model recommended by Launder and Spalding[9] were used in the present work without any modification, which are C_1=1.44, C_2=1.92, C_μ= 0.09, σ_k=1 and σ_ε =1.3.

2.2 MULTIPHASE FLOW MODELING: THE EULERIAN-EULERIAN SOLUTION METHOD

The Eulerian-Eulerian model has been used to represent the multiphase flow during the atomization process considering a three-phase system, where air, water and liquid steel are present. The Eulerian-Eulerian approach treats each phase as continuum and solves continuity, momentum and energy equations for each phase[10].

To begin with, the volume fraction indicates the space occupied by each phase and the law of conservation of mass and the conservation of momentum are satisfied by each individual phase. The volume of the phase p is denoted by V_p and is defined as following,

$$V_p = \int_V \alpha_p dV \qquad \text{Equation 7}$$

Where α_p stands for the plastic volume and the total volume fraction in the computational cell remains one.

Furthermore, the continuity equation for the phase q is shown below,

$$\frac{\partial}{\partial t}(\alpha_q \rho_q) + \nabla\cdot(\alpha_q \rho_q \vec{v}_q) = \sum_{p=1}^{n}(\dot{m}_{pq} - \dot{m}_{qp}) + S_q \qquad \text{Equation 8}$$

In Equation 8, the velocity of phase q is given by $\vec{v}_q$ and $\dot{m}_{pq}$ is characterized by the mass transfer from p^{th} to q^{th} phase and $\dot{m}_{qp}$ is the mass transfer from phase q to phase p. S_q is the source term.

Lastly, the momentum balance for the phase q is given by the following,

$$\frac{\partial}{\partial t}(\alpha_q \rho_q \overrightarrow{v_q}) + \nabla\cdot(\alpha_q \rho_q \overrightarrow{v_q}\,\overrightarrow{v_q}) = -\alpha_q \nabla p + \nabla\cdot\bar{\bar{\tau}}_q + \sum_{p=1}^{n}(\overrightarrow{R_{pq}} + \dot{m}\,\overrightarrow{v_{pq}} - \dot{m}_{qp}\,\overrightarrow{v_{pq}}) + (\overrightarrow{F_q} + \vec{F}_{lift,q} + \vec{F}_{vm,q}) \qquad \text{Equation 9}$$

Where $\overrightarrow{F_q}$, $\vec{F}_{lift,q}$ and $\vec{F}_{vm,q}$ indicate an external body force, a lift force and a virtual mass force

respectively. $\overrightarrow{R_{pq}}$ is an interaction force between phases and the pressure is given by p, that is shared by all phases.

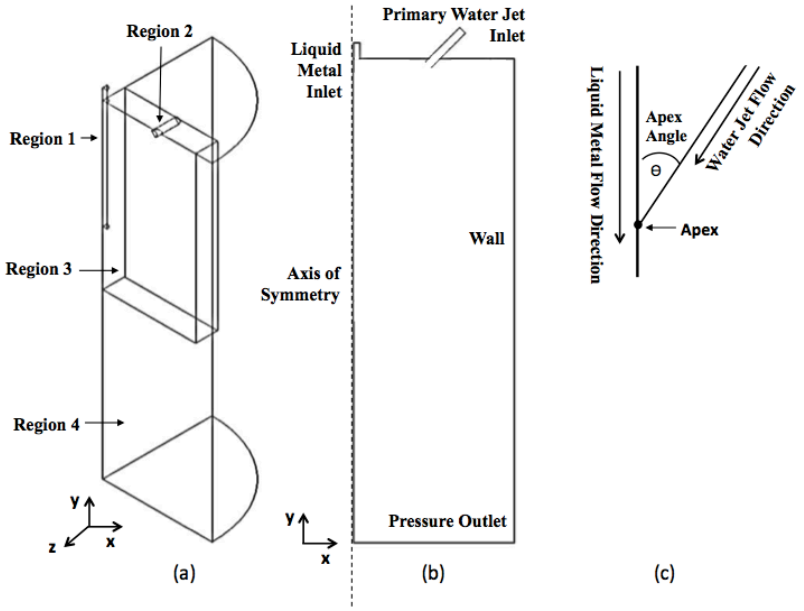

Figure 2. (a) The geometrical illustration of the water atomizer. (b) The computational domain of the water atomizer and boundary conditions. (c) The definition of apex and apex angle.

2.3 GRID GENERATION

The schematic representation of a v-jet water atomizer employed in the present work is shown in **Figure *2***. The 3D model was built asymmetrically along the center of the liquid steel stream due to the symmetrical configuration of the water atomizer. As shown in **Figure *2*** (b), the axis of symmetry was placed on the left side of the computational domain. The primary water nozzle and tundish nozzle were located at the top of the domain while the water outlet was placed at the bottom. The grid was generated using two different element types. Fine quadrilateral elements were employed near the two nozzle regions that are Region 1 and 2 in **Figure *2***(a) and coarse hexagonal dominant grid was applied to the rest of the atomization chamber (Region 3 and 4). The entire computation domain consisted of approximately 280,000 cells. As can be seen in **Figure *2***(c), the apex angle is defined as the angle in between the liquid steel stream and the water jets while the point of contact is named as apex.

2.4 BOUNDARY CONDITIONS

Both the liquid steel and water nozzle inlets were set as pressure inlet condition while the atomization chamber outlet was considered as a pressure outlet. The atmospheric pressure was used as the outlet pressure. The center line of the liquid steel flow was set to be the axis of symmetry, and the other boundaries were set as stationary walls.

3.0 RESULTS AND DISCUSSION

As mentioned earlier, the present work is dedicated in investigating the effect of the apex angle, the water nozzle design and the metal nozzle diameter during the atomization process. Thus, 3D CFD simulations were performed in various cases as shown in **Table *II***.

Table II: Summary of various simulation cases done in the present work.

	Apex Angle Study					Water Speed Study			Water Inlet Diameter Study			Liquid Steel Inlet Diameter Study			
Apex Angle (°)	15	20	25	35	45	20			20			20			
Water Speed (m/s)	140					110	140	170	140			140			
Water Inlet Diameter (mm (inch))	10 (0.39)					10 (0.39)			8 (0.31)	10 (0.039)	12 (0.47)	10 (0.039)			
Metal Inlet Diameter (mm (inch))	16 (0.63)					16 (0.63)			16 (0.63)			12 (0.47)	16 (0.63)	20 (0.79)	24 (0.94)
Melt Flow Rate (m/s)	3.5														

3.1 INFLUENCE OF APEX ANGLE

Momentum transfer is the basic underlying mechanism during the process of water atomization, where liquid steel gets disintegrated upon the impact from water jets[11]. In **Figure *3***(a), kinetic energies of within the impact zone (Region 1 in **Figure *2*** (a)) were plotted against various apex angles. With the increase in the apex angle, a significant increased amount of mean flow kinetic energy and turbulence kinetic energy were transferred to the liquid steel stream, which facilitate the disintegration of the liquid steel. Moreover, in water atomization, droplet formation was mostly influenced by impact phenomenon rather than shear as recorded in Equation 10[12]. In this equation, it can be noticed that the mass median particle size of the atomized powder is proportional to the water velocity that is normal to the liquid steel flow direction. Consequently, finer particles were produced at higher apex angle when water jet velocity stayed constant.

$$d_{50} = \frac{C_3}{v_w \sin\theta} \qquad \text{Equation 10}$$

Where d_{50}, C_3, v_w and θ stand for mass median particle size of atomized powder, model constant, water velocity and apex angle respectively. Here w is the subscript in representation of water jet.

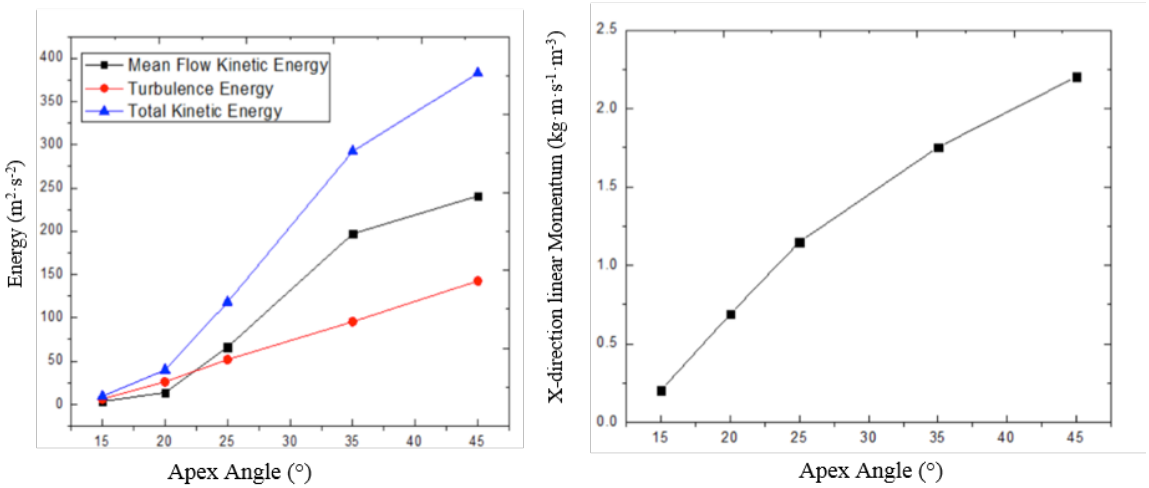

Figure 3. (a) Calculated mean flow kinetic energy, turbulence kinetic energy and total kinetic energy in the impact zone at various apex angles during water atomization. (b) Calculated X-direction momentum of water in the impact zone at various apex angles

Such correlation can be further explained based on the conservation of momentum. For simplicity, it was assumed that the water droplets transferred all of its momentum M_w to the newly atomized metal particle with a unit momentum of M_m. Therefore, when a single water droplet struck the liquid steel stream surface and resulted in n number of formed metal particles, one can write the momentum balance equation as

$$M_w = nM_m \qquad \text{Equation 11}$$

Considering the case of one individual spherical metal particle with diameter of d^i, velocity v^i and density of ρ. Equation 11 can be rearranged as

$$d_m^i = d_w^i\left(\frac{v_w\rho_w}{nv_m\rho_m}\right)^{\frac{1}{3}} \qquad \text{Equation 12}$$

If the median diameter of the metal particle was considered here, Equation 12 became,

$$d_m = d_w\left(\frac{v_w\rho_w}{nv_m\rho_m}\right)^{\frac{1}{3}} \qquad \text{Equation 13}$$

This momentum model indicated that metal particle size is a function of two unknown parameters d_w and v_w. Let the diameter of the water droplet remain constant, the correlation between X-direction of water momentum ($v_{x,w}\rho_w$) with respect to various apex angles was given in **Figure *3***(b). More specifically, at a higher apex angle, the momentum transfer in the direction that is normal to the liquid steel flow direction (seen in **Figure *4***b) was higher. Therefore, finer particles were produced at high apex angle.

However, the increase in apex angle also gave rise to the risk of premature solidification (often referred to as freeze-up) in the near-nozzle region[13]. With the increase in apex angle, the position of apex moved closer and closer to the liquid steel inlet as demonstrated in **Figure *4***(b). In **Figure *5***, the volume fractions of the liquid steel and the vector velocity filed of the water jet during atomization at different apex angles were plotted. When the apex angle reached 35 degrees, it can be noticed that the atomizing water started moving upward towards the liquid steel inlet. Consequently, the liquid steel was constrained within the near-nozzle region by a large kinetic force from the water jet, which greatly increased the chance of premature solidification and water welled-up in that region. Although, as discussed previously, higher apex angles lead to smaller particle sizes, an improper design would eventually lead to a trade off of

powder disintegration efficiency, which influenced the final characteristics of the powder. In the previous study carried out by J.J. Dunkley[4], 50 degrees was suggested as a practical limit to the magnitude of the apex angle because of the incidence of liquid metal freeze-up at the nozzle. In other words, powder size control via increasing the apex angle should be considered as a dangerous unstable practice. It is better to obtain a stable setup configuration with minimum rejection of the metal towards the metal inlet nozzle, and then by tuning other operation parameters such as water jet velocity to achieve finer particle size.

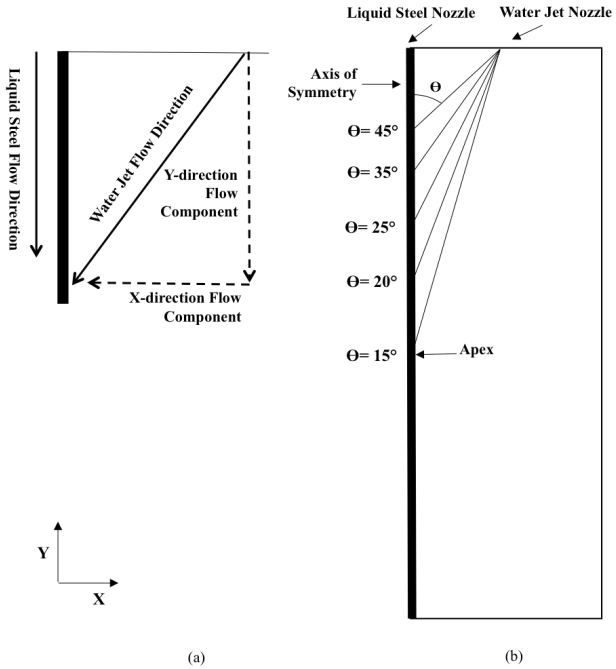

Figure 4. (a) the locations of apex with respect to various apex angles. (b) Schematic of water jet flow vector.

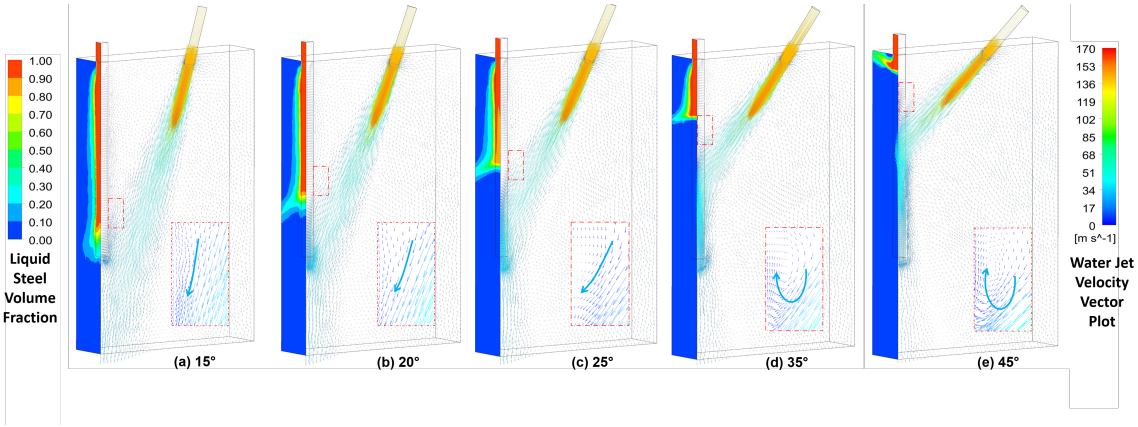

Figure 5. Volume fraction contour plot of the liquid steel and the water jet velocity vector plot at various apex angles: (a) 15° (b) 20° (c) 25° (d) 35° (e) 45°. The regions highlighted in the red are zoomed-in velocity vector plot. The blue arrows indicate the domain velocity vectors in different cases.

3.2 INFLUENCE OF WATER NOZZLE DESIGN

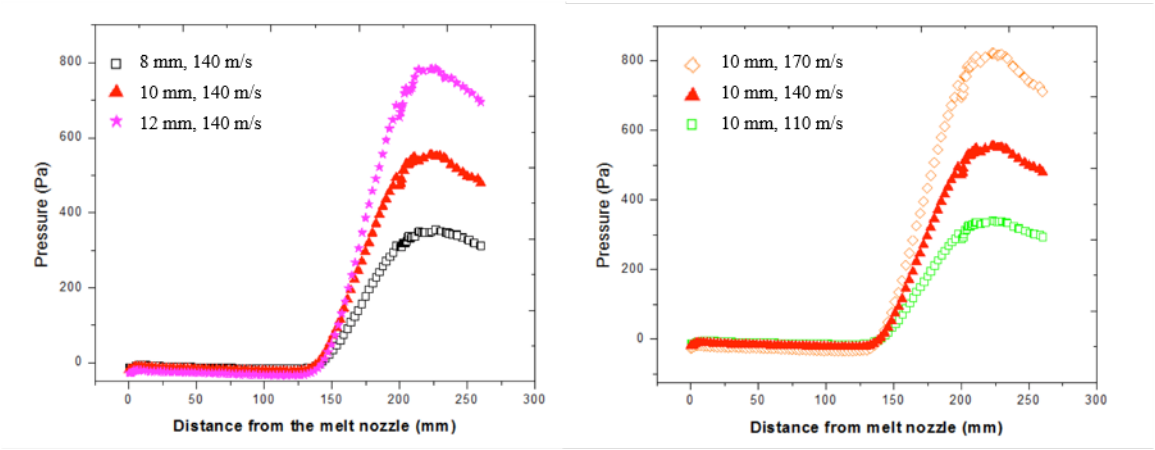

Figure 6. Static pressure curve along the central axis of the liquid steel flow field: (a) Various water nozzle diameters with the same water jet flow rate (b) Various water jet flowrate with the same water nozzle diameter

Water nozzle diameter and water jet flowrate were two primary variables considered in nozzle design. In **Figure *6***a, the effect of nozzle diameter and water flowrate on the static pressure along the centerline of the liquid steel flow were given and appeared to be rather similar. More specifically, with the increase in both parameters, there was a larger static pressure at the liquid steel- water jet interface. Furthermore, a static pressure gradient is presented along the centerline of the liquid steel flow and this gradient increased as the water nozzle diameter or the water jet flowrate increased. Such pressure gradient gave insight for the processes of liquid sheet breakup.

Based on various studies[14], droplet formation in atomization maybe roughly classified into the following phenomenon: a) liquid dripping; b) liquid jet break breakup; c) liquid ligament breakup d) liquid sheet/film breakup and e) liquid free-surface break. During the atomization, the pressure gradient gives rise to the liquid steel flow to deform and spread, which results in a thin liquid steel film along the direction of the flow. Upon the interaction with the incoming water jet, the thin liquid metal film subsequently goes through the primary breakup and formed ligaments and sheets. These ligaments and sheets are then spheroidized driven by the surface tension of the film and became large metal droplets. It is well established that the size of the droplets depended to a large extent on the thickness of the liquid sheet[15]. When the liquid steel sheet is thicker, the size of the liquid steel droplets produced by primary break becomes bigger. On the other hand, the thickness of the liquid steel flow is known to be inversely proportional to the pressure gradient along the centerline of the liquid steel. In other words, a larger pressure gradient gives rise to a thinner liquid steel film. As a result, large pressure gradient caused by increased water inlet diameter or water flowrate may lead to fine liquid steel particles formed during primary breakup. It can also be noted that at higher water flowrate (170 m/s) and larger water inlet nozzle diameter (12 mm, 0.47 inch), no rising pattern of the liquid steel, similar to **Figure *5***(d), was observed in the current study. This suggested that water flow velocity and diameter might be the safe choices of parameters to adjust during atomization to satisfy specific customer demand.

3.3 INFLUENCE OF METAL INLET DIAMETER

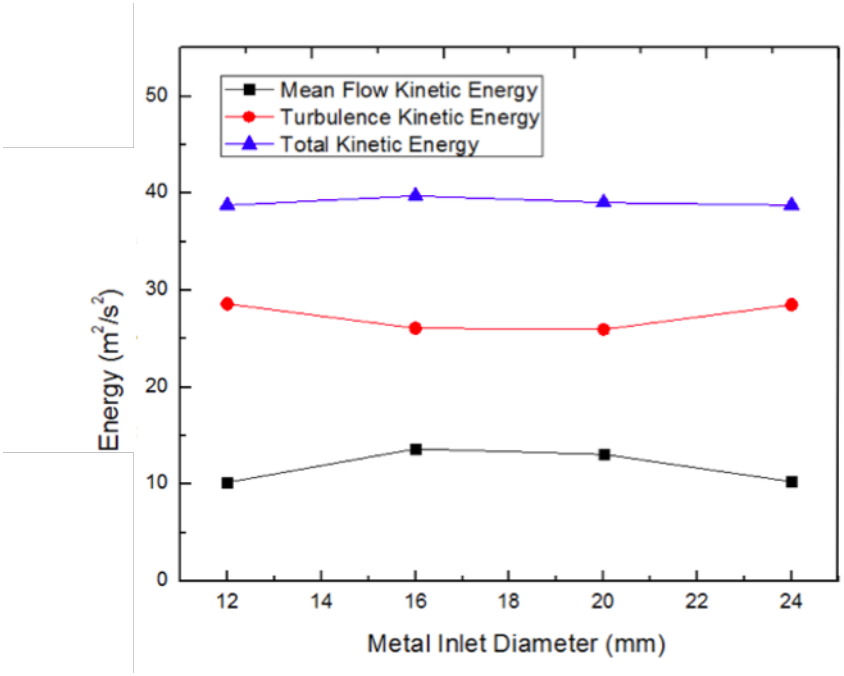

Figure 7. Mean Flow Kinetic Energy, Turbulence Kinetic Energy and Total Kinetic Energy obtained over various metal inlet diameters: 12 mm (0.47 inch), 16 mm (0.63 inch), 20 mm (0.79 inch) and 24 mm (0.94 inch).

Various simulations were performed to study how the liquid steel inlet diameter can influence kinetic energy transfer. The metal inlet diameter is directly related to the liquid steel flow rate where a larger inlet diameter allows more liquid steel enter the atomization chamber per unit time. The liquid steel flow rate was calculated using Equation 14.

$$\text{liquid steel Flowrate} = \rho \cdot v_{M,} \cdot A \qquad \text{Equation. 14}$$

Where ρ, v_M and A_M are the liquid steel density, velocity and the liquid steel inlet cross-sectional area.

In the previous study[1], no appreciable influence of liquid steel inlet diameter was observed since there was no major change in resultant mean flow kinetic energy, which was an influential factor in disintegrating the liquid steel as discussed previously. Therefore, within the range of liquid steel inlet diameters considered in the present work, the effect of liquid steel inlet diameter on particle size was found to be negligible. This finding aliened with multiple studies in the past. For example, J.J. Dunkley et al[4] reported that no significant effect on particle size was observed by increasing the water flow-to-metal flow ratio. Furthermore, Equation 15 was the model developed by Bergquist on estimating the d_{50} value of as atomized power[16],

$$d_{50} = C_3 \frac{\gamma_M^{0.8} \mu_M}{P_W^{0.8} \sin\theta} \left(\frac{m_w}{m_m}\right)^{-0.043} \qquad \text{Equation 15}$$

Where C_3 is the model constant, γ_m is the surface tension of the liquid metal (N m^{-1}), μ_m is the viscosity of the liquid metal (Pa s), P_w is the water pressure (Pa), θ is the apex angle, m_m and m_m (kg s^{-1}) are the mass flowrates of the water and liquid metal respectively.

As shown in the model, in the case of present work, the only changing variable is the liquid steel flowrate. The exponent -0.043 indicates a rather modest increase on d_{50} by increasing the liquid steel flow rate. In

practice, the increase in the liquid steel flow rate can also be caused by several other parameters besides the cross-sectional change in the liquid steel stream, like freezing or wear of liquid steel nozzle and the height of liquid metal in the tundish etc. Although an increase in liquid steel flowrate is a viable option to augment the capacity of the atomizer, it should not be achieved at the cost of the powder quality due to the insufficient impinging power from the water jets in respect to the increase liquid steel flowrate.

4.0 CONCLUSIONS

A three dimensional numerical model has been developed to simulate the water atomization process under various design configurations and operation parameters using ANSYS FLUNET 16.2. To begin with, the result has shown that the apex angle has an important influence on kinetic energy and momentum in between the water jet and the liquid steel stream. At a larger apex angle, more x-direction linear momentum was transferred, which can facilitate the disintegrations of the liquid steel stream and the formation of finer-sized droplets. By increasing the water jet diameter or the water flowrate, a higher static pressure gradient was obtained along the centerline of the liquid steel flow. Subsequently, a thinner liquid steel sheet/film was produced which is known to result in smaller droplet diameter. Lastly, within the range of the present work performed on the liquid steel inlet diameter, its effect on kinetic energy transfer and droplet size was negligible. Going forward, physical modeling will be performed to verify the current findings along with more extensive simulations exploring a wider range of process parameters.

LIST OF SYMBOLS

d_{50} mass median particle diameter of the atomized powder
k kinetic energy
C_3 model constant
v velocity
θ apex angle
M momentum
d^i individual spherical metal particle diameter
ρ density
n number of metal particles formed per one droplet of water
A cross-section area
γ surface tension
μ viscosity
P pressure
m mass flow rate

SUBSCRIPT

m liquid metal
w water

REFERENCE

[1] M. Schmidt and K. Rohrbach, "ASM Handbook, Volume 1: Properties and Selection: Irons, Steels, and High-Performance Alloys," *Met. Handb.*, vol. 1, pp. 793–800, 1990.

[2] F. Persson, A. Eliasson, and P. Jönsson, "Prediction of particle size for water atomised metal powders: parameter study List of symbols."

[3] S. S and B. T.J., "No Title," *Int. J. Powder Metall.*, vol. 4, no. 3, pp. 7–17, 1968.

[4] J. J. Dunkley and J. D. Palmer, "Factors affecting particle size of atomized metalpowders," *Powder Metall.*, vol. 29, pp. 287–290, 1986.

[5] Y. Seki, O. S, T. H, and N. Kawai, "No Title," *Met. Powder Rep.*, vol. 45, no. 1, pp. 38–40, 1990.

[6] A. T. Ankus and R. D. Venter, "No Title," *Powder Technol.*, vol. 73, no. 2, pp. 169–179, 1992.

[7] T. H. Wang, W. H. Lee, and W. C. Liu, "China Steel technical report no. 7," 1993.

[8] Y. F. Ternovoi and O. S. Nichiporenko, "No Title," *Poroshk. Met.*, vol. 1, pp. 1–7, 1993.

[9] B. E. Launder and D. B. Spalding, "The numerical computation of turbulent flow," *Comput. Methods Appl. Mech. Eng.*, vol. 3, no. 2, pp. 269–289, 1974.

[10] *ANSYS-Fluent 15.0 Theory Guide*, vol. 15317, no. November. Southpointe, 2013.

[11] A. J. Aller and A. Losada, "Models in the Metal Powders Atomization," *Powder Metall. Sci. Technol.*, vol. 2, no. 2, pp. 13–37, 1991.

[12] R. J. Grandzol and J. A. Tallmadge, "Effect of jet angle on water atomization," *Int. J. Powder Metall. Powder Technol.*, vol. 11, no. 2, pp. 103–116, 1975.

[13] P. C. Angelo and R. Subramanian, *Powder Metallurgy: Science, Technology and Applications*. PHI Learning Pvt. Ltd., 2008.

[14] H. Liu, *Science and Engineering of Droplets: Fundamentals and Applications*. 1981.

[15] A. H. Lefebvre, *Gas Trubine Conbustion*. Washington.D.C. USA, 1983.

[16] B. Bergquist, *Powder Metall.*, vol. 42, pp. 331–343, 1999.